Salomäki, Janne; Hinkkanen, Marko; Luomi, Jorma

Cost-effective design of inverter output filters for AC drives

Published in:
The 33rd Annual Conference of the IEEE Industrial Electronics Society (IECON'07)

DOI:
10.1109/IECON.2007.4459927

Published: 05/11/2007

Document Version
Peer-reviewed accepted author manuscript, also known as Final accepted manuscript or Post-print

Please cite the original version:
Salomäki, J., Hinkkanen, M., & Luomi, J. (2007). Cost-effective design of inverter output filters for AC drives. In *The 33rd Annual Conference of the IEEE Industrial Electronics Society (IECON'07)* (pp. 1220-1226). https://doi.org/10.1109/IECON.2007.4459927

Cost-Effective Design of Inverter Output Filters for AC Drives

Janne Salomäki, Marko Hinkkanen, and Jorma Luomi
Power Electronics Laboratory
Helsinki University of Technology
P.O. Box 3000, FI-02015 TKK, Finland

***Abstract*— The paper deals with the minimization of output filter cost in inverter-fed AC drives. The LC filter design is constrained by the total harmonic distortions of the stator voltage and inverter output current, the voltage drop in the filter inductor, and the system resonance frequency. The last constraint is important from the control point of view, because the vector control requires that the sampling frequency is sufficiently higher than the resonance frequency. The design takes into account the frequency dependence of the filter resistance and inductance due to the eddy currents in the laminated iron-core inductor. The design method is further enhanced by taking into account the inverter power stage cost as a function of the switching frequency. The design minimizes the total cost of the inverter and filter, and determines the optimal switching frequency. Simulations and experiments show that the filter designed according to the proposed design procedure fulfils the design constraints, and the speed-sensorless control works well with the cost-optimized filter.**

I. Introduction

Pulse-width modulated variable-speed drives have become common in many industrial and household applications. Besides many advantages such as energy savings and good controllability, frequency converters have also brought along some unwanted effects. The output voltage of the inverter consists of sharp-edged voltage pulses, which may cause excessive voltage stresses in the stator winding insulations of the motor. They may also give rise to leakage currents through the parasitic capacitances of the stator winding and produce bearing currents. Lower-order harmonics cause acoustic noise and power losses in the motor.

A means to overcome these problems is using a sinusoidal inverter output filter (or a sine-wave filter) [1]. As additional advantages, the filter may bring along cost savings in other components of the drive system: (i) the inverter can be rated smaller because a part of the magnetizing current is fed by the filter capacitors [2]; (ii) unshielded cables can be used if the common-mode voltage is filtered [3]; (iii) the grid side EMI filter can be avoided [4]. Conventionally, the drives equipped with a sinusoidal output filter are based on constant volts-per-hertz control. However, the control performance can be improved by using sensorless vector control [5], [6]. If vector control is used, the sampling frequency should be sufficiently higher than the resonance frequency of the filter, which sets a constraint for the filter design.

The design of a sinusoidal filter is usually based on the resonance frequency of the filter [2], [7]–[9]. The resonance frequency has been set one decade below the switching frequency in [9]. However, to minimize the filter cost, the resonance frequency should be closer to the switching frequency. In [10], [11], the relative cost of the inductor and capacitor (based on an estimate that the capacitor cost is half of the inductor cost for the same power rating [12]) is taken into account in the filter design.

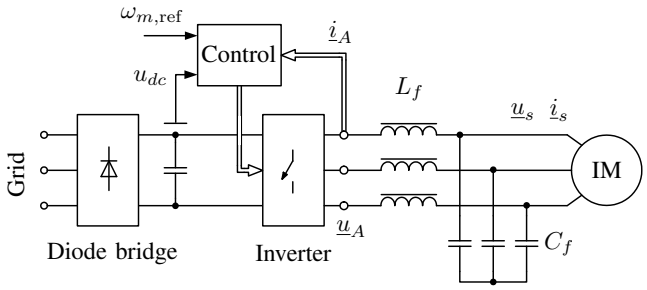

Fig. 1. Variable-speed drive system equipped with inverter output filter.

Laminated iron-core inductors are usually used in sinusoidal output filters. Due to the eddy currents in the laminations, the resistance and the inductance of the filter inductor depend significantly on the frequency. Hence, a frequency-dependent inductor model should be applied in the filter design, especially if the switching frequency is high.

In this paper, a cost-effective design of a sinusoidal output filter for vector-controlled drive is developed. The filter cost is based on present-day component prices. The design is constrained by the total harmonic distortion (THD) of the stator voltage, the THD of the inverter output current, and the voltage drop in the filter inductor. Furthermore, the maximum resonance frequency is constrained by the sampling frequency in the case of vector-controlled drives. The cost of the filter is minimized so that given filtering requirements are fulfilled. In addition, the optimal switching frequency is determined in order to minimize the total cost of the filter and the power stage of the inverter. The design is verified by simulations and experiments.

II. Filter and Motor Models

Fig. 1 shows the variable-speed drive system equipped with an inverter output filter. Space-vector notation is used for three-phase quantities. The inverter output voltage $\underline{u}_A$ is filtered by an LC filter, and the induction motor (IM) is fed

by the filtered voltage $\underline{u}_s$. The inverter output current and the stator current are denoted by $\underline{i}_A$ and $\underline{i}_s$, respectively.

The state-space representation of the system, consisting of the LC filter and the induction motor, can be written as

$$\frac{\mathrm{d}\underline{\mathbf{x}}}{\mathrm{d}t} = \underline{\mathbf{A}}\,\underline{\mathbf{x}} + \mathbf{B}\underline{u}_A \tag{1}$$

where $\underline{\mathbf{x}} = \begin{bmatrix}\underline{i}_A & \underline{u}_s & \underline{i}_s & \underline{\psi}_R\end{bmatrix}^T$ is the state vector. The matrix transpose is denoted by the superscript T and the rotor flux linkage is $\underline{\psi}_R$. The system matrices in stationary coordinates are

$$\underline{\mathbf{A}} = \begin{bmatrix} -\frac{R_{Lf}}{L_f} & -\frac{1}{L_f} & 0 & 0 \\ \frac{1}{C_f} & 0 & -\frac{1}{C_f} & 0 \\ 0 & \frac{1}{L'_s} & -\frac{1}{\tau'_\sigma} & \frac{1}{L'_s}(\frac{1}{\tau_r} - j\omega_m) \\ 0 & 0 & R_R & -\frac{1}{\tau_r} + j\omega_m \end{bmatrix} \tag{2}$$

$$\mathbf{B} = \begin{bmatrix}\frac{1}{L_f} & 0 & 0 & 0\end{bmatrix}^T \tag{3}$$

where L_f is the inductance and R_{Lf} the series resistance of the filter inductor, C_f is the capacitance of the filter, and ω_m is the electrical angular speed of the rotor. Corresponding to the inverse-Γ model of the induction motor [13], R_s and R_R are the stator and rotor resistances, respectively, L'_s is the stator transient inductance, and L_M the magnetizing inductance. The two time constants are defined as $\tau'_\sigma = L'_s/(R_s + R_R)$ and $\tau_r = L_M/R_R$.

At higher frequencies, the variation of the filter inductance with the frequency should be modeled. Because of the skin and proximity effects, the leakage inductance of an inductor decreases and the winding resistance increases with frequency. These changes depend on the wire and winding dimensions, and they can be reduced by proper winding design. As the frequency increases above several kilohertz, the eddy currents induced in the laminated iron core start to decrease the main inductance of an inductor. In the following, analytical expressions are used for modeling the behavior of the iron core [14]. For simplicity, the effects of magnetic saturation are ignored, and so are the skin and proximity effects in the windings. The series resistance and inductance of the inductor are given by

$$R_{Lf} = R_{Lf,\mathrm{dc}} + \omega L_{f,\mathrm{dc}} \frac{\delta}{w} \frac{\sinh\frac{w}{\delta} - \sin\frac{w}{\delta}}{\cosh\frac{w}{\delta} + \cos\frac{w}{\delta}} \tag{4}$$

$$L_f = L_{f,\mathrm{dc}} \frac{\delta}{w} \frac{\sinh\frac{w}{\delta} + \sin\frac{w}{\delta}}{\cosh\frac{w}{\delta} + \cos\frac{w}{\delta}} \tag{5}$$

respectively, where $R_{Lf,\mathrm{dc}}$ and $L_{f,\mathrm{dc}}$ are the dc resistance and dc inductance of the filter inductor, respectively, $\delta = \sqrt{2\rho/(\mu\omega)}$ is the skin depth of the iron sheet , ρ is the electrical resistivity of the iron sheet, μ is the magnetic permeability, ω is the angular frequency, and w is the thickness of a single sheet.

III. Harmonic Analysis of Inverter Output Voltage

The inverter output voltage reference having the angular frequency ω_s is modulated with a carrier signal having the angular frequency ω_c. The spectrum of the resulting switching voltage $u_a(t)$ can be determined analytically by means of a double Fourier series expansion [15]:

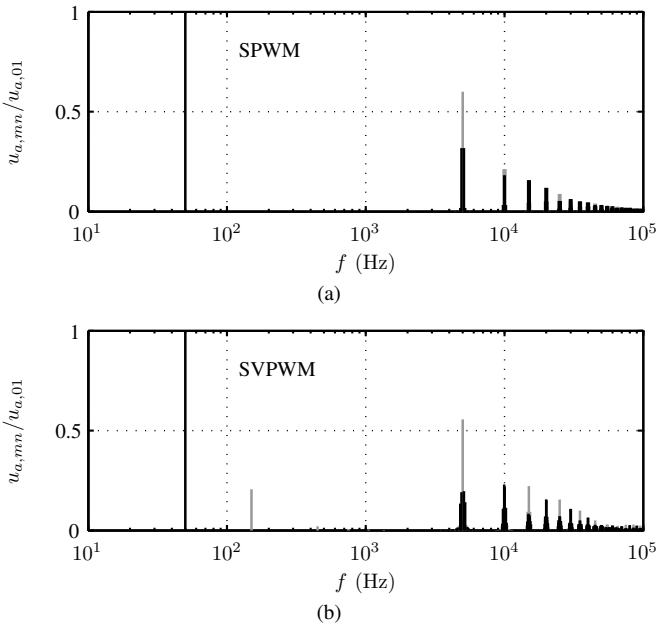

Fig. 2. Theoretical spectra of inverter switching voltage when $\omega_c = 2\pi \cdot 5000$ rad/s, $\omega_s = 2\pi \cdot 50$ rad/s, and $M_d = 1$ for (a) SPWM and (b) SVPWM. The zero-sequence components are shown as grey bars.

$$u_a(t) = \sum_{m=-\infty}^{\infty} \sum_{n=-\infty}^{\infty} \underline{u}_{a,mn} e^{j(m\omega_c + n\omega_s)t} \tag{6}$$

The coefficients are given by the double integral:

$$\underline{u}_{a,mn} = \frac{1}{T_c T_s} \int_0^{T_c} \int_0^{T_s} u_a(t) e^{-j(m\omega_c + n\omega_s)t} dt\, dt \tag{7}$$

where $T_c = 2\pi/\omega_c$ ja $T_s = 2\pi/\omega_s$.

Different modulation methods produce different harmonic spectra for the inverter output voltage. When the classical sinusoidal PWM (SPWM) is used, the Fourier coefficients of the switching voltage u_a are [16]:

$$\underline{u}_{a,mn} = \frac{u_{dc}}{m\pi} J_n\left(\frac{M_d \pi m}{2}\right) \sin\left[\frac{(m+n)\pi}{2}\right] \tag{8}$$

where u_{dc} is the dc-link voltage, $M_d = 2|\underline{u}_A|/u_{dc}$ is the modulation depth, and J_n is an nth-order Bessel function. Fig. 2(a) shows the theoretical spectrum of an example switching voltage generated by the SPWM.

The spectrum of the PWM voltage generated by symmetrical suboscillation or the corresponding space vector PWM (SVPWM) is more complicate to calculate analytically. The solution is presented in [17]. Fig. 2(b) shows the theoretical spectrum of an example switching voltage generated by the SVPWM.

In a three-phase system, zero-sequence components disappear from phase to phase and space vector voltages. The space vector of the inverter output voltage can be expressed as a double Fourier series expansion:

$$\underline{u}_A(t) = \sum_{m=-\infty}^{\infty} \sum_{n=-\infty}^{\infty} \underline{u}_{A,mn} e^{j(m\omega_c + n\omega_s)t} \tag{9}$$

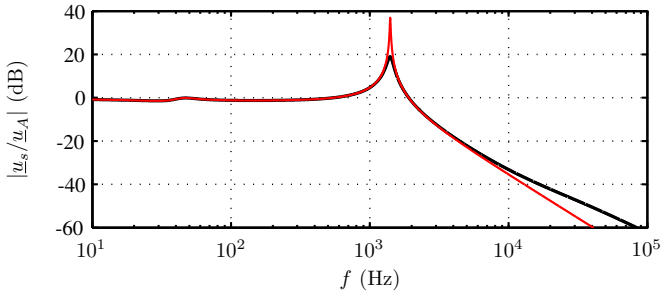

Fig. 3. Amplitude-frequency response from $\underline{u}_A$ to $\underline{u}_s$ when frequency-dependent inductor model is used (thick line) and when inductor parameters are constant: $L_f = L_{f,\mathrm{dc}}$ and $R_{Lf} = R_{Lf,\mathrm{dc}}$ (thin line).

where the Fourier coefficients $\underline{u}_{A,mn}$ are obtained from the coefficients of the switching voltage as

$$\underline{u}_{A,mn} = \frac{2}{3}\left[1 + e^{j(1-n)2\pi/3} + e^{j(1-n)4\pi/3}\right]\underline{u}_{a,mn} \quad (10)$$

The derivation of (10) is given in the Appendix.

IV. Filtering Characteristics

Based on (1)–(3), the transfer function from the inverter output voltage to the stator voltage is

$$\underline{G}(s) = \frac{\underline{u}_s(s)}{\underline{u}_A(s)} = \begin{bmatrix}0 & 1 & 0 & 0\end{bmatrix}(s\mathbf{I} - \underline{\mathbf{A}})^{-1}\underline{\mathbf{B}} \quad (11)$$

where $\mathbf{I}$ is a 4×4 identity matrix. Similarly, the transfer function from the inverter output voltage to the inverter output current can be expressed as

$$\underline{Y}(s) = \frac{\underline{i}_A(s)}{\underline{u}_A(s)} = \begin{bmatrix}1 & 0 & 0 & 0\end{bmatrix}(s\mathbf{I} - \underline{\mathbf{A}})^{-1}\underline{\mathbf{B}} \quad (12)$$

Fig. 3 shows the frequency response (11) at the nominal angular speed of an example motor. The motor parameters are given in Table I. The filter parameters used in this example are $L_{f,\mathrm{dc}} = 3.8$ mH, $C_f = 4.0$ µF, and $R_{Lf,\mathrm{dc}} = 0.3\ \Omega$. The parameters of the iron core are $\rho = 7\cdot10^{-7}\ \Omega$m, $\mu = 300\mu_0$, and $w = 0.5$ mm. The resonance frequency of the system depends on the filter parameters and also on the stator transient inductance according to

$$f_{\mathrm{res}} = \frac{1}{2\pi\sqrt{C_f\frac{L_f L'_s}{L_f + L'_s}}} \quad (13)$$

The filter resistance damps the LC resonance. If the inverter output voltage does not include harmonics near the resonance frequency, the internal resistance of the filter inductor is usually sufficient, and no separate damping resistor is needed.

A. Total Harmonic Distortion of Stator Voltage

The Fourier coefficients of the stator voltage vector $\underline{u}_s$ are

$$\underline{u}_{s,mn} = \underline{G}_{mn}\underline{u}_{A,mn} \quad (14)$$

TABLE I
Parameters of the 2.2-kW Four-Pole 400-V 50-Hz Induction Motor and the Voltage Source Inverter

Motor Parameters	
Stator resistance R_s	3.67 Ω
Rotor resistance R_R	1.65 Ω
Stator transient inductance L'_s	0.021 H
Magnetizing inductance L_M	0.264 H
Total moment of inertia J	0.0155 kgm^2
Rated speed n_N	1430 r/min
Rated current (rms) I_N	5.0 A
Rated torque T_N	14.6 Nm
Inverter Parameters	
DC-link voltage u_{dc}	540 V
Switching frequency f_c	5 kHz
Sampling frequency f_{sa}	10 kHz

where $\underline{G}_{mn} = \underline{G}(s)|_{s=j(m\omega_c+n\omega_s)}$. Using these Fourier coefficients related to space vectors, the root-mean square (rms) phase-to-neutral stator voltage becomes

$$U_s = \sqrt{\frac{1}{2}\sum_{m=-\infty}^{\infty}\sum_{n=-\infty}^{\infty}|\underline{u}_{s,mn}|^2} \quad (15)$$

All carrier and sideband harmonics are taken into account even if they are not a multiple of ω_s. The filtering performance can be evaluated by means of the total harmonic distortion (THD) of the stator voltage:

$$\mathrm{THD}_{us} = \frac{\sqrt{U_s^2 - U_{s1}^2}}{U_{s1}} \quad (16)$$

where $U_{s1} = |\underline{u}_{s,01}|/\sqrt{2}$ is the rms fundamental component of $\underline{u}_s$.

B. Voltage Drop

The voltage drop over the filter inductor at the fundamental frequency should be small. The relative voltage drop can be calculated as

$$k_{\Delta u} = \frac{U_{A1} - U_{s1}}{U_{A1}} \quad (17)$$

where $U_{A1} = |\underline{u}_{A,01}|/\sqrt{2}$ is the rms fundamental component of $\underline{u}_A$. The voltage drop depends not only on the filter inductance, but also on the filter capacitance.

C. Total Harmonic Distortion of Inverter Current

The rms inverter output current is

$$I_A = \sqrt{\frac{1}{2}\sum_{m=-\infty}^{\infty}\sum_{n=-\infty}^{\infty}|\underline{i}_{A,mn}|^2} \quad (18)$$

where $\underline{i}_{A,mn} = \underline{Y}_{mn}\underline{u}_{A,mn}$ and $\underline{Y}_{mn} = \underline{Y}(s)|_{s=j(m\omega_c+n\omega_s)}$. When an LC filter is used, the inverter output current harmonics increase because the filter capacitor provides a low-impedance route for high-frequency currents. These currents are limited mainly by the filter inductor. The THD of the inverter output current can be calculated as

$$\mathrm{THD}_{iA} = \frac{\sqrt{I_A^2 - I_{A1}^2}}{I_{A1}} \quad (19)$$

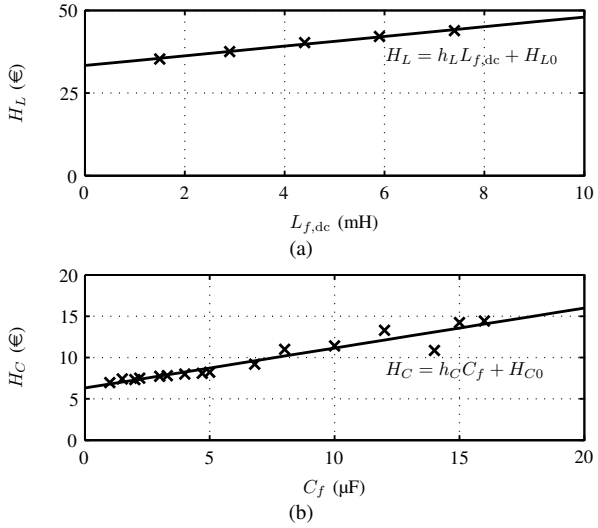

Fig. 4. Filter component prices: (a) Three-phase inductor (5 A), (b) Capacitor (450 V). Price parameters are $h_L = 1.47$ €/mH, $H_{L0} = 33.3$ €, $h_C = 0.48$ €/µF, and $H_{C0} = 6.3$ €.

where $I_{A1} = |\underline{i}_{A,01}|/\sqrt{2}$ is the rms fundamental component of $\underline{i}_A$.

V. Cost-Effective Filter Design

A. Cost Function

Fig. 4 shows example component prices for LC filters. The inductor and capacitor prices, denoted by H_L and H_C, respectively, can be approximated by linear functions. The trend line drawn in Fig. 4(a) is reasonable only for inductors having the same current rating. Capacitor prices shown in Fig. 4(b) are for a constant rated voltage. The cost function consists of the inductor and capacitor prices according to

$$H_{\mathrm{filter}} = h_L L_{f,\mathrm{dc}} + H_{L0} + 3\Big(h_C C_f + H_{C0}\Big) \qquad (20)$$

where h_L, H_{L0}, h_C, and H_{C0} are price parameters that define the trend lines in Fig. 4.

B. Filter Design

The filter design problem can be formulated as a constrained optimization problem

$$\min_{L_{f,\mathrm{dc}}, C_f} H_{\mathrm{filter}} \qquad (21)$$

such that

$$\mathrm{THD}_{us} \le \mathrm{THD}_{us,\max} \qquad (22)$$

$$\mathrm{THD}_{iA} \le \mathrm{THD}_{iA,\max} \qquad (23)$$

$$k_{\Delta u} \le k_{\Delta u,\max} \qquad (24)$$

$$f_{\mathrm{res}} \le f_{\mathrm{res,max}} \qquad (25)$$

where $\mathrm{THD}_{us,\max}$ is the maximum allowed THD of the stator voltage, $\mathrm{THD}_{iA,\max}$ is the maximum allowed THD of the inverter current, and $k_{\Delta u,\max}$ is the maximum allowed relative voltage drop in the filter inductor. The last constraint (25) is important from the control point of view. The vector control of the drive system with an LC filter requires that the sampling frequency f_{sa} is sufficiently higher than the resonance frequency f_{res} of the system. According to various simulations with an example drive, the sampling frequency should be at least four times the resonance frequency.

Especially THD_{iA} and $k_{\Delta u}$ vary with the operating point significantly. Therefore, the filter design constraints should be determined according to the desired operating point. The nominal operating point of the drive is typically chosen for the filter design.

The motor and inverter parameters given in Table I are used in the following design example. The constraints for the example design are given in Table II. The modulation method is the SVPWM. A nominal operating point of the drive is defined by $M_d = 2/\sqrt{3}$, $\omega_s = 2\pi \cdot 50.0$ rad/s, and $\omega_m = 2\pi \cdot 47.7$ rad/s. The dc resistance of the filter inductor is assumed to be $R_{Lf,\mathrm{dc}} = 0.3\ \Omega$. The optimization task (21)–(25) is solved using the *fmincon* function of the MATLAB Optimization Toolbox.

Fig. 5 shows a contour plot of the cost function and the constraint curves. The feasible region lies above each constraint curve. The optimal filter design is obtained at point A ($L_{f,\mathrm{dc}} = 3.4$ mH, $C_f = 3.5$ µF), where the cost is $H_{\mathrm{filter}} = 62.2$ €.

In the previous design, the sampling frequency was twice the switching frequency. If the sampling frequency equals the switching frequency as is the case in some drives, the feasible region shrinks according to the dashed line in Fig. 5. The resonance frequency of the system must be lower than that in the previous design in order to fulfil the constraint (25). In this case, the optimal filter design is obtained at point B ($L_{f,\mathrm{dc}} = 4.0$ mH, $C_f = 4.8$ µF), where the cost is $H_{\mathrm{filter}} = 65.1$ €.

TABLE II
Filter Design Constraints

$\mathrm{THD}_{us,\max}$	4 %
$\mathrm{THD}_{iA,\max}$	20 %
$k_{\Delta u,\max}$	3 %
$f_{\mathrm{res,max}}$	$0.25 \cdot f_{\mathrm{sa}} = 2.5$ kHz

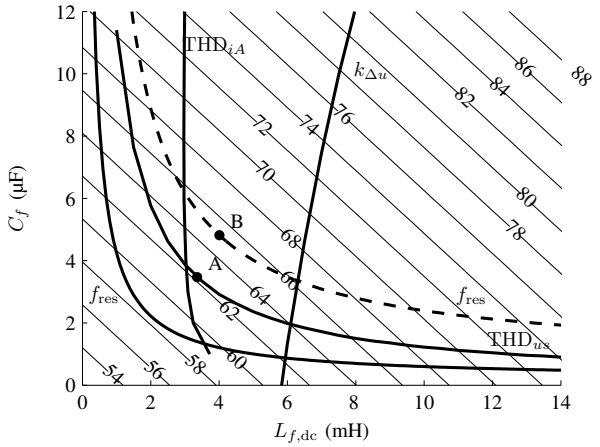

Fig. 5. Optimal filter design. Point A is the optimal design if $f_{\mathrm{sa}} = 2f_c$. Point B is the optimal design if $f_{\mathrm{sa}} = f_c$.

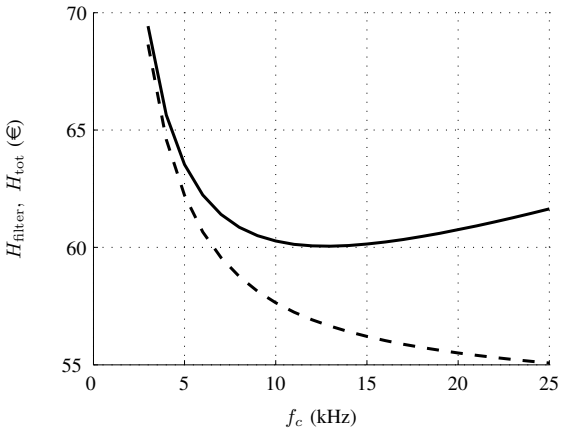

Fig. 6. Cost as function of switching frequency. Dashed line is the filter component cost $H_{\rm filter}$. Solid line is the total cost of the filter components and inverter oversizing.

C. Effect of Switching Frequency

The filter design in the previous subsection is optimal only for a fixed switching frequency. By solving the optimization problem (21)–(25) for different switching frequencies (assuming $f_{\rm sa} = 2f_c$), the effect of the switching frequency can be investigated. Fig. 6 shows the filter component cost (dashed line) as a function of the switching frequency. The increase of the inverter switching frequency results in decreased inductance and capacitance of the filter. Consequently, smaller and cheaper components can be used.

A higher switching frequency, however, causes higher switching losses in the inverter. The switching losses may require oversizing of the inverter. The cost of the oversized inverter can be taken into account in the filter design in a fashion similar to [18] for a grid-side LCL filter. The aim is to minimize the total cost of the filter and the power stage of the inverter. The results give the optimal filter parameters and the optimal switching frequency.

The inverter switching losses with sinusoidal currents can be approximated as [19]

$$P_{\rm sw} = \frac{6}{\pi} f_c (E_{\rm on,T} + E_{\rm off,T} + E_{\rm off,D}) \frac{u_{dc}}{u_{\rm ref}} \frac{|i_A|}{i_{\rm ref}} \qquad (26)$$

where $E_{\rm on,T}$ and $E_{\rm off,T}$ are the turn-on and turn-off energies of the IGBT, respectively, and $E_{\rm off,D}$ is the turn-off energy of the diode. The switching energies are provided in data sheets for a certain blocking state voltage $u_{\rm ref}$ and a reference current $i_{\rm ref}$. According to (26), the switching losses of the inverter are linearly proportional to the switching frequency. The ratio of the switching losses to the switching frequency is denoted by $p_{\rm sw} = P_{\rm sw}/f_c$. The total cost is obtained by adding the inverter oversizing cost to the filter component cost (20):

$$H_{\rm tot} = H_{\rm filter} + h_{\rm ov} p_{\rm sw} f_c \qquad (27)$$

where $h_{\rm ov}$ is an inverter oversizing cost factor.

The parameters used in (27) are $p_{\rm sw} = 3.3$ W/kHz and $h_{\rm ov} = 0.08$ €/W in this example design. The total cost is shown as a function of the switching frequency in Fig. 6 (solid line). The minimum total cost is obtained at $f_c = 13$ kHz. The corresponding filter parameters are $L_{f,\rm dc} = 1.6$ mH and $C_f = 1.4$ µF, and the filter cost is $H_{\rm filter} = 56.6$ €.

VI. Simulation Results

The drive system equipped with the cost-optimized filter was investigated by computer simulations using the MATLAB/Simulink software. The frequency dependence of the filter inductance and resistance was not included in the simulation model. The motor and inverter parameters given in Table I were used with the exception of $f_{\rm sa} = 5$ kHz. The filter parameters were $L_f = 4$ mH, $C_f = 4.8$ µF, and $R_{Lf} = 0.3\ \Omega$ corresponding to the optimal filter design in Fig. 5 (point B). A speed-sensorless control method [5] enhanced with a one-step-ahead current prediction in the inverter current control was used. The bandwidths of the controllers were $2\pi \cdot 700$ rad/s for the inverter current, $2\pi \cdot 466$ rad/s for the stator voltage, $2\pi \cdot 233$ rad/s for the stator current, and $2\pi \cdot 7.5$ rad/s for the rotor speed.

Fig. 7 shows simulation results. The speed reference was set to $\omega_{m,\rm ref} = 0.95$ p.u. at $t = 0.5$ s. A rated load step was applied at $t = 1.5$ s and removed at $t = 2.5$ s. Finally, the drive was decelerated to standstill. According to the test sequence the control works well with the cost-optimized filter.

Fig. 8 shows voltage and current waveforms at a speed of $\omega_{m,\rm ref} = 0.95$ p.u. under rated load torque. The spectrum of the stator voltage is plotted in Fig. 11(a). The LC filter attenuates high frequencies from the inverter output voltage effectively. The THD of the stator voltage is $\rm THD_{us} = 2.1\ \%$, the THD of the inverter current is $\rm THD_{iA} = 14.3\ \%$, and the voltage drop is $k_{\Delta u} = 1.9\ \%$. All constrains given in Table II are fulfilled.

VII. Experimental Results

The experimental setup consists of a frequency converter controlled by a dSPACE DS1103 PPC/DSP board, a 2.2-kW four-pole induction motor, and a three-phase LC filter. The parameters of the motor and the inverter correspond to those given in Table I with the exception of $f_{\rm sa} = 5$ kHz and $u_{dc} = 520$ V. The LC filter consists of a three-legged laminated iron-core inductor and three AC capacitors. The technical data of the filter is given in Table III. A permanent magnet servo motor was used as loading machine. Only the dc-link voltage and the inverter output current were measured for control purposes. The stator voltage, the stator current, the rotor flux linkage, and the rotor speed were estimated by means of an adaptive full-order observer as described in [5]. The rotor speed was measured only for monitoring purposes. Simple current feedforward compensation for dead times and power device voltage drops was applied [20]. The inverter output voltage was limited to $0.98u_{dc}/\sqrt{3}$ in order to reduce oscillations due to the minimum pulse-width limitation of the inverter.

Fig. 9 presents the experimental results corresponding to the simulation shown in Fig. 7. The measured control

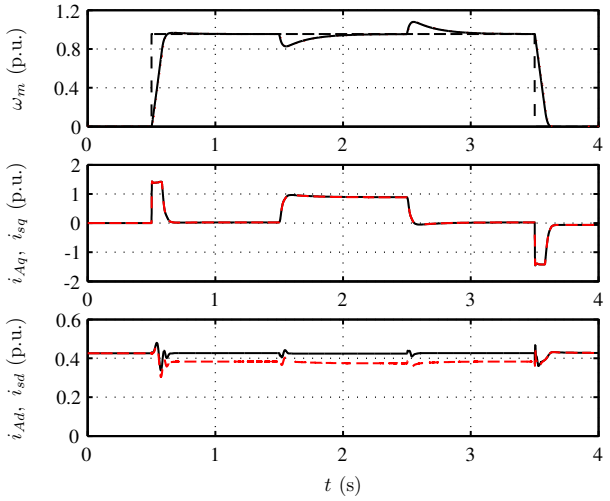

Fig. 7. Simulation results showing speed and load changes. The first subplot shows the rotor speed (solid), its reference (dashed), and its estimate (dotted). The second subplot shows the q-axis components of the stator current (solid) and the inverter output current. The third subplot shows the d-axis components of the stator current (solid) and the inverter output current.

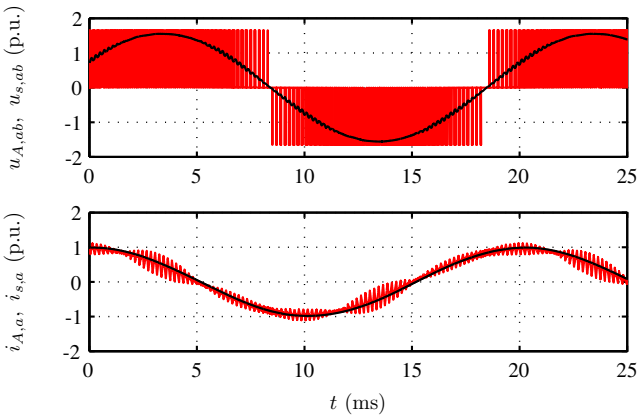

Fig. 8. Simulation results showing voltage and current waveforms. The first subplot shows the inverter output voltage (phase to phases) and the stator voltage (phase to phases). The second subplot shows the inverter output current and the stator current.

TABLE III
TECHNICAL DATA OF THE LC FILTER

3-phase inductor	Muuntosähkö Trafox 3INP5 50145
Inductance	3 x 4.0 mH
Rated voltage	400 V
Rated current	5.0 A
Capacitor	3 x EPCOS B25832-F4505-K001 MKV
Capacitance	5.0 µF ±10 %
Rated voltage	640 V

performance corresponds well to the simulation results. The oscillations in the inverter output current are caused by inverter nonidealities and measurement inaccuracies.

Fig. 10 shows voltage and current waveforms at a speed of $\omega_{m,\mathrm{ref}} = 0.95$ p.u. under rated load torque. The spectrum of the stator voltage is plotted in Fig. 11(b). Inverter nonidealities and measurement inaccuracies cause harmonics between the fundamental frequency and the switching frequency. The

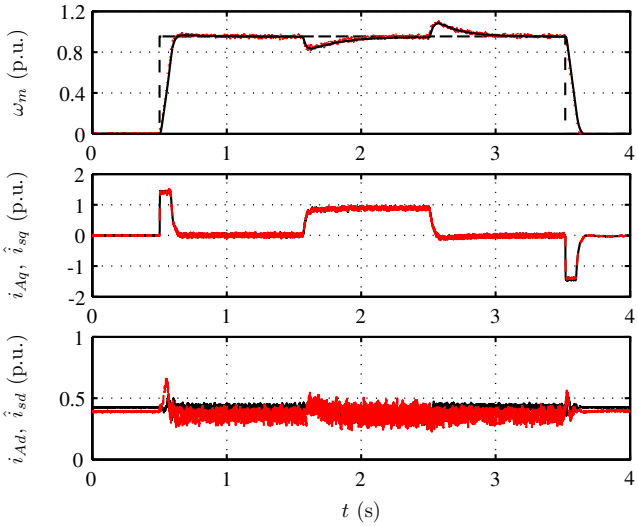

Fig. 9. Experimental results showing a sequence with speed and load changes. The explanations of the curves are as in Fig. 7. Estimated values are shown for the stator current.

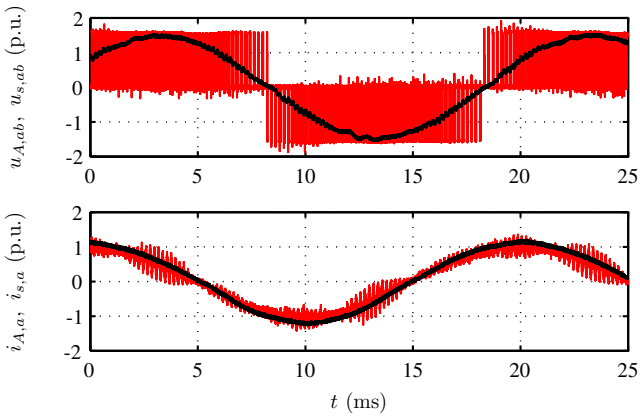

Fig. 10. Experimental results showing voltage and current waveforms. The explanations of the curves are as in Fig. 8.

filter amplifies the harmonics around the system resonance frequency of 1.2 kHz. The amplitudes of the switching frequency harmonics are of the same order of magnitude as those in the simulation. The THD of the stator voltage is $\mathrm{THD}_{us} = 3.6$ %, the THD of the inverter current is $\mathrm{THD}_{iA} = 18.1$ %, and the voltage drop is $k_{\Delta u} = 1.3$ %. The THD of the stator voltage is higher than that obtained in the simulation. This difference is explained by inverter nonidealities and measurement inaccuracies, which were not taken into account in the simulation nor in the filter design. However, all constrains given in Table II are fulfilled.

VIII. CONCLUSION

A cost-effective design of inverter output filters requires knowledge of filter component prices, motor and inverter parameters, and filtering requirements. If the drive is vector controlled, the sampling frequency should be at least four times the resonance frequency of the system. This requirement can be a limiting factor especially if the sampling frequency is low. Otherwise, the limiting factor can be the

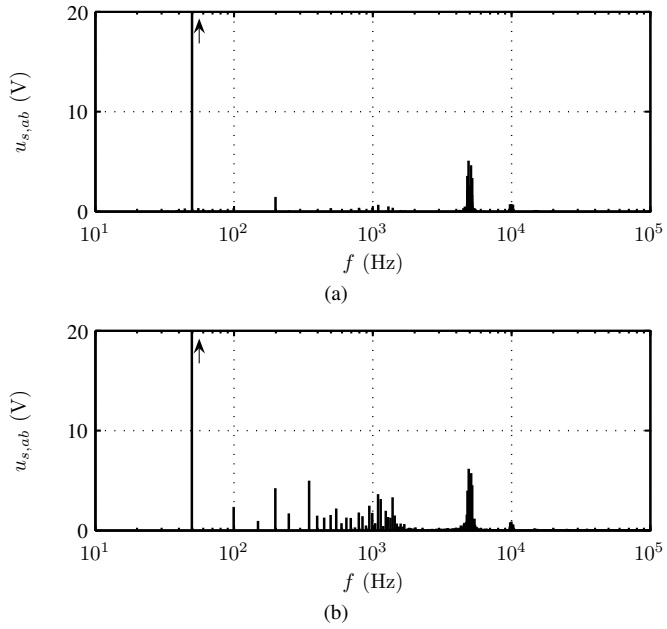

Fig. 11. (a) Simulation and (b) experimental results showing spectrum of stator voltage (phase to phase). The amplitude of the fundamental component is beyond the scale of the figure.

THD of the stator voltage or the THD of the inverter output current. The voltage drop can be the dominant constraint if the fundamental frequency is high. The inverter power stage cost can be taken into account in the filter design in order to find the optimal switching frequency. The increase of the switching frequency reduces the filter price, but the inverter cost is increased due to higher switching losses. Simulation and experimental results show that the filter designed according to the proposed design procedure fulfils the design constraints, and the speed-sensorless vector control works well with the cost-optimized filter.

ACKNOWLEDGMENT

The authors would like to thank ABB Oy, the Finnish Foundation of Technology, and the KAUTE Foundation for the financial support.

APPENDIX
FOURIER COEFFICIENTS OF SPACE VECTOR VOLTAGE

The Fourier series of the switching voltages in each three phases are

$$u_a(t) = \sum_{m=-\infty}^{\infty} \sum_{n=-\infty}^{\infty} \underline{u}_{a,mn} e^{j(m\omega_c + n\omega_s)t} \tag{28}$$

$$u_b(t) = \sum_{m=-\infty}^{\infty} \sum_{n=-\infty}^{\infty} \underline{u}_{a,mn} e^{j[(m\omega_c + n\omega_s)t - 2\pi n/3]} \tag{29}$$

$$u_c(t) = \sum_{m=-\infty}^{\infty} \sum_{n=-\infty}^{\infty} \underline{u}_{a,mn} e^{j[(m\omega_c + n\omega_s)t - 4\pi n/3]} \tag{30}$$

The space vector of the inverter output is

$$\underline{u}_A = \frac{2}{3}\left(u_a + u_b e^{j2\pi/3} + u_c e^{j4\pi/3}\right) \tag{31}$$

Substituting (28)–(30) in (31) results in

$$\underline{u}_A(t) = \sum_{m=-\infty}^{\infty} \sum_{n=-\infty}^{\infty} \underbrace{\frac{2}{3}\left[1 + e^{j(1-n)2\pi/3} + e^{j(1-n)4\pi/3}\right] \underline{u}_{a,mn}}_{\underline{u}_{A,mn}} e^{j(m\omega_c + n\omega_s)t} \tag{32}$$

where $\underline{u}_{A,mn}$ are the Fourier coefficients of the space vector voltage.

REFERENCES

[1] P. T. Finlayson, "Output filters for PWM drives with induction motors," *IEEE Ind. Applicat. Mag.*, vol. 4, no. 1, pp. 46–52, Jan./Feb. 1998.

[2] J. Huppunen and J. Pyrhönen, "Filtered PWM-inverter drive for high-speed solid-rotor induction motors," in *Conf. Rec. IEEE-IAS Annu. Meeting*, vol. 3, Rome, Italy, Oct. 2000, pp. 1942–1949.

[3] N. Hanigovszki, J. Landkildehus, G. Spiazzi, and F. Blaabjerg, "An EMC evaluation of the use of unshielded motor cables in AC adjustable speed drive applications," *IEEE Trans. Power Electron.*, vol. 21, no. 1, pp. 273–281, Jan. 2006.

[4] N. Hanigovszki, "EMC output filters for adjustable speed drives," Ph.D. dissertation, Inst. Energy Techn., Aalborg Univ., Aalborg, Denmark, Mar. 2005.

[5] J. Salomäki, M. Hinkkanen, and J. Luomi, "Sensorless control of induction motor drives equipped with inverter output filter," *IEEE Trans. Ind. Electron.*, vol. 53, no. 4, pp. 1188–1197, Aug. 2006.

[6] J. Salomäki, A. Piippo, M. Hinkkanen, and J. Luomi, "Sensorless vector control of PMSM drives equipped with inverter output filter," in *Proc. IEEE IECON'06*, Paris, France, Nov. 2006, pp. 1059–1064.

[7] H. Akagi, H. Hasegawa, and T. Doumoto, "Design and performance of a passive EMI filter for use with a voltage-source PWM inverter having sinusoidal output voltage and zero common-mode voltage," *IEEE Trans. Power Electron.*, vol. 19, no. 4, pp. 1069–1076, July 2004.

[8] J. K. Steinke, "Use of an LC filter to achieve a motor-friendly performance of the PWM voltage source inverter," *IEEE Trans. Energy Conversion*, vol. 14, no. 3, pp. 649–654, Sep. 1999.

[9] H. van der Broeck and C. Loef, "Use of LC filters in hard switching PWM inverter drives," in *Proc. EPE'95*, Sevilla, Spain, Sep. 1995.

[10] P. Wheeler and D. Grant, "Optimised input filter design and low-loss switching techniques for a practical matrix converter," *IEE Proc.-Electr. Power Appl.*, vol. 144, no. 1, pp. 53–60, Jan. 1997.

[11] C. Xiyou, Y. Bin, and G. Yu, "The engineering design and the optimization of inverter output RLC filter in AC motor drive system," in *Proc. IEEE IECON'02*, Sevilla, Spain, Nov. 2002, pp. 175–180.

[12] F. Brichant, *Force-Commutated Inverters: Design and Industrial Applications*. Oxford, UK: North Oxford Academic, 1984.

[13] G. R. Slemon, "Modelling of induction machines for electric drives," *IEEE Trans. Ind. Applicat.*, vol. 25, no. 6, pp. 1126–1131, Nov./Dec. 1989.

[14] G. Grandi, M. K. Kazimierczuk, A. Massarini, U. Reggiani, and G. Sancineto, "Model of laminated iron-core inductors for high frequencies," *IEEE Trans. Magn.*, vol. 40, no. 4, pp. 1839–1845, July 2004.

[15] H. S. Black, *Modulation Theory*. New York, NY: Van Nostrand, 1953.

[16] S. R. Bowes and M. I. Mech, "New sinusoidal pulsewidth-modulated invertor," *Proc. IEE*, vol. 122, no. 11, pp. 1279–1285, 1975.

[17] J. F. Moynihan, M. G. Egan, and J. M. D. Murphy, "Theoretical spectra of space-vector-modulated waveforms," *IEE Proc. Electr. Power Appl.*, vol. 145, no. 1, pp. 17–24, Jan. 1998.

[18] P. Peltoniemi, "Comparison of vector modulation methods and output filters of a grid-connected voltage source converter," Master's thesis, Dept. Elect. Eng., Lappeenranta Univ. Tech., Lappeenranta, Finland, 2005, in Finnish.

[19] U. Nicolai, T. Reimann, J. Petzoldt, and J. Lutz, *Application Manual Power Modules*. Ilmenau, Germany: Verlag ISLE, 2000.

[20] J. K. Pedersen, F. Blaabjerg, J. W. Jensen, and P. Thøgersen, "An ideal PWM-VSI inverter with feedforward and feedback compensation," in *Proc. EPE'93*, vol. 4, Brighton, U.K., Sept. 1993, pp. 312–318.